



Fabrication of Magnetic Chitosan-Benzil Biopolymer with Organoclay for Remazol Brilliant Blue R Dye Removal: a Statistical Modeling and Adsorption Mechanism

Ali H. Jawad^{1,2,3} · Ahmed Saud Abdulhameed^{4,5} · Ahmad Hapiz^{1,2} · Salis Awal Musa^{1,2} · Ruihong Wu^{1,2,6} · Zeid A. ALOthman⁷

Received: 30 March 2024 / Accepted: 1 May 2024

© The Author(s), under exclusive licence to Springer Science+Business Media, LLC, part of Springer Nature 2024

Abstract

In this work, a magnetic cross-linked chitosan-benzil/organoclay/Fe₃O₄ biocomposite (CHI-BZI/OC/Fe₃O₄) was synthesized as a bio-adsorbent for the removal of remazol brilliant blue R (RBBR) dye from aquatic environment. The adsorption factors i.e., CHI-BZI/OC/Fe₃O₄ dosage, pH, and time were statistically optimized using the Box-Behnken design (BBD). The highest RBBR removal efficiency of 90.9% was achieved at a CHI-BZI/OC/Fe₃O₄ dosage of 0.1 g/100 mL, initial solution pH of 4.0, and contact time of 20 min. The RBBR adsorption onto the CHI-BZI/OC/Fe₃O₄ matched the pseudo-second-order kinetic (PSO). Moreover, equilibrium study was conducted and the best fit to the adsorption experimental data was described by Langmuir isotherm model. The adsorption capacity of CHI-BZI/OC/Fe₃O₄ for RBBR was determined to be 102.9 mg/g. This work contributes to the advancement of environmentally friendly and sustainable methods for treating dye-contaminated water, showcasing the potential of biocomposite materials as effective adsorbents in the field of water purification.

Keywords Chitosan · Crosslinking · Benzil · Organoclay · Statistical Modeling

1 Introduction

Synthetic dyes are widely used in industrial sectors such as pharmaceuticals, textile, cosmetics, and plastic industries, resulting in the generation of effluents contaminated with dyes [1, 2]. These wastewaters reduce sunlight penetration, interfere with photosynthesis, and increase chemical oxygen demand as well as negatively impact the aquatic environment [3]. Additional health dangers from exposure to organic dyes include increased heart rate, allergic responses, respiratory tract irritation, and nausea [4]. To protect the ecology and promote water reuse, it is necessary to purify water that has become contaminated with these hazardous chemicals. For the removal of dyes from polluted wastewater, a variety of techniques have been explored such as adsorption [5–7], ion exchange [8], nanofiltration [9], biological degradation [10], and Fenton oxidation [11]. Among these, the adsorption technique has gained popularity due to the availability of different adsorbents, simple preparation, easy handling, low operational cost, and high efficiency [12].

Chitosan (CHI) is a non-toxic, biodegradable, and linear cationic polymer that is obtained from chitin deacetylation [13]. CHI is an attractive adsorbent for water remediation

✉ Ali H. Jawad
ali288@uitm.edu.my; ahjm72@gmail.com

¹ Faculty of Applied Sciences, Universiti Teknologi MARA, 40450 Shah Alam, Selangor, Malaysia

² Advanced Biomaterials and Carbon Development Research Group, Faculty of Applied Sciences, Universiti Teknologi MARA, 40450 Shah Alam, Selangor, Malaysia

³ Environmental and Atmospheric Sciences Research Group, Scientific Research Center, Al-Ayen University, Thi-Qar, Nasiriyah 64001, Iraq

⁴ Department of Pharmaceutical Chemistry, College of Pharmacy, University of Anbar, Ramadi, Iraq

⁵ College of Engineering, University of Warith Al-Anbiyaa, Karbala, Iraq

⁶ Department of Chemistry, Hengshui University, 053500, Hebei Province, Hengshui, China

⁷ Chemistry Department, College of Science, King Saud University, 11451 Riyadh, Saudi Arabia

due to its unique properties [14]. It can interact with a variety of contaminants owing to its amine and hydroxyl functional groups [15]. However, unmodified CHI has some limitations for use in wastewater treatment. It is soluble in acidic environments and has a high swelling index [16]. To overcome these limitations, CHI can be modified physicochemically. This can involve crosslinking, grafting, or other methods to improve its solubility, swelling index, and adsorption capacity [17].

Covalent cross-linking is a common approach for improving the physical and chemical characteristics of CHI [18]. Cross-linking agents are used to create covalent connections with the functional groups of CHI, resulting in stronger and more stable cross-linked CHI [19]. However, common cross-linking agents like formaldehyde, glutaraldehyde, and glyoxal have been found to reduce the adsorption ability of CHI [20]. To overcome this limitation, alternative cross-linking molecules with plenty of chemical groups are desirable. Benzil (BZI), which contains phenyl rings, is one such substitute. The introduction of phenyl rings through the use of BZI leads to the formation of a more intricate network that has an enhanced affinity for organic dyes. This is because BZI contains conjugated systems of phenyl rings that can interact with the aromatic system of organic dyes through π - π stacking interactions [21].

The utilization of CHI composite adsorbents has emerged as a promising approach to enhance adsorption capabilities [22]. These composites offer improved selectivity, regeneration potential, surface area, mechanical strength, and surface chemistry compared to conventional materials [19]. Among the various composite options, chitosan-organoclay biocomposites have garnered considerable interest [23]. The exceptional sorption behavior and large specific surface area of organoclays make them particularly suitable for adsorbing hydrophobic organic compounds and ionic pollutants, further enhancing their appeal as efficient adsorbents in environmental applications [24–26]. Thus, by combining the advantageous properties of both organic and inorganic components, these biocomposites exhibit a versatile range of characteristics like environmentally friendly, adsorption ability, and chemical stability [27]. Recently, researchers have started investigating the possibility of employing magnetic adsorbents based on biocomposites for wastewater treatment [28]. This novel technique entails the development of biomagnetic derivatives of CHI, which have distinct benefits in the removal of contaminants from water [29]. These biomagnetic adsorbents are famous for their capacity to be readily recovered and separated from mixtures via an external magnetic field, removing the need for traditional filtering processes [30].

Thus, the primary goal is to develop a multi-functional adsorbent of a cross-linked chitosan-benzil/organoclay/ Fe_3O_4 biocomposite (CHI-BZI/OC/ Fe_3O_4). The focus of

this biocomposite is to achieve efficient adsorptive removal of RBBR dye from aqueous environments. To achieve this objective, the present study employed the Box-Behnken design (BBD) to statistically optimize the adsorption experimental data. The obtained data were further validated using analysis of variance (ANOVA) to ensure the reliability and significance of the results. The experimental findings from the adsorption process were also fitted with different kinetic and isotherm models. Furthermore, the study aims to propose a comprehensive mechanism for RBBR adsorption using the CHI-BZI/OC/ Fe_3O_4 .

2 Materials and methods

2.1 Materials

CHI (deacetylation degree of $\geq 75\%$) and BZI were obtained from Sigma-Aldrich. Organoclay was obtained from HmbG and Bendosen Laboratory. Iron (II) chloride tetrahydrate ($\text{FeCl}_2 \cdot 4\text{H}_2\text{O}$) and iron (III) chloride hexahydrate ($\text{FeCl}_3 \cdot 6\text{H}_2\text{O}$) were acquired from HmbG and Bendosen Laboratory Chemicals. Acidic RBBR dye (MW of 626.54 g/mol, λ_{max} of 595 nm, and chemical structure is given in Fig.S1) was purchased from ACROS, Organics. All the chemical compounds were of analytical quality and utilized without additional purification in the tests.

2.2 Preparation of CHI-BZI/OC/ Fe_3O_4

This paragraph describes the method used to prepare the CHI-BZI/OC/ Fe_3O_4 adsorbent for use in the removal of synthetic textile dye RBBR. Initially, a 50 mL solution of 5% acetic acid was combined with 1 g of CHI flakes and 1 g of OC, and the mixture was agitated at a high RPM for 24 h to allow for complete CHI dissolution. Then, 10 mL of distilled water was combined with $\text{FeCl}_3 \cdot 6\text{H}_2\text{O}$ and $\text{FeCl}_2 \cdot 4\text{H}_2\text{O}$, and the resultant mixture was transferred to the CHI/OC solution and agitated for an hour. The viscous solution was injected into a 1000 mL NaOH solution (2 M) with a syringe needle while being gently stirred, and CHI/OC/ Fe_3O_4 beads started to form right away. To eliminate any remaining sodium hydroxide solution, the beads were then rinsed with distilled water. After that, the CHI/OC/ Fe_3O_4 beads were crosslinked by adding 100 mL of 2% BZI and letting them sit in a water bath shaker at 40 °C for two hours. The CHI-BZI/OC/ Fe_3O_4 beads were dried after being rinsed with distilled water to create tiny particles ($\sim 250 \mu\text{m}$). The end product was employed for adsorption experiments to evaluate its efficacy in removing RBBR synthetic textile dye. The details of employed technologies to characterize the CHI-BZI/OC/ Fe_3O_4 were outlined in the supplementary material (Table S1).

Table 1 Codes and actual variables and their levels in BBD

Codes	Variables	Level 1 (-1)	Level 2 (0)	Level 3 (+1)
A	CHI-BZI/OC/ Fe ₃ O ₄ dose (g/100 mL)	0.02	0.06	0.1
B	pH	4	7	10
C	Time (min)	5	25	35

2.3 Box-Behnken Design

Box-Behnken Design (BBD) model was chosen for investigating the influence of variables on the adsorption of RBBR onto CHI-BZI/OC/Fe₃O₄ from an aqueous system. The BBD model considers the impact of individual or mutual interaction of factors. The Design-Expert software (v 13, Stat-Ease) was used to perform adsorption tests and present the results graphically. The process parameters of CHI-BZI/OC/Fe₃O₄ dose (A), pH (B), and contact time (C) were selected as input variables, while the RBBR removal (%) was the response (Y). The levels range of factors in BBD are given in Table 1. Second-order expression (Eq. 1) was used to explain the link between the response variable and independent factors.

$$Y = \beta_0 + \sum \beta_i X_i + \sum \beta_{ii} X_i^2 + \sum \beta_{ij} X_i X_j \quad (1)$$

In this equation, Y stands for the response optimization (RBBR removal, %), X_i and X_j are the examined factors, and β_0 and β_i , β_{ii} , and β_{ij} , respectively, are constant coefficients, coefficients of linear effects, coefficients of quadratic effects, and coefficients of interaction effects. Table 2 presents the BBD matrix and the corresponding RBBR removal (%) values. To start the experiment, a specific amount of CHI-BZI/OC/Fe₃O₄ was added to 100 mL of RBBR solution with fixed concentration (50 mg/L) in Erlenmeyer flasks of volume 250 mL. The flasks were then agitated using a water bath shaker at a speed of 85 rpm. Then, CHI-BZI/OC/Fe₃O₄ was separated from the mixtures using an external magnetic bar, and a 0.45 μ m syringe filter was then applied. The spectrophotometer (HACH DR 3800) was used to measure the concentrations of RBBR at λ_{\max} of 595 nm. Equation (2) was used to obtain the efficiency of RBBR removal (%).

$$R\% = \frac{(C_o - C_e)}{C_o} \times 100 \quad (2)$$

where the initial RBBR concentration (mg/L) is C_o and the equilibrium concentration (mg/L) of RBBR is C_e .

2.4 Batch Adsorption Experiment

A batch adsorption system was used to investigate the removal of RBBR using a biocomposite-based adsorbent of CHI-BZI/OC/Fe₃O₄. Table 2 showed that the highest

Table 2 Matrix of BBD model and the related response (RBBR removal (%))

Run	A:CHI-BZI/OC/ Fe ₃ O ₄ (g)	B:pH	C:Time (min)	RBBR removal (%)
1	0.02	4	20	29.9
2	0.1	4	20	90.9
3	0.02	10	20	27.9
4	0.1	10	20	72.1
5	0.02	7	5	11.4
6	0.1	7	5	46.1
7	0.02	7	35	24.3
8	0.1	7	35	86.5
9	0.06	4	5	20.8
10	0.06	10	5	27.7
11	0.06	4	35	68.2
12	0.06	10	35	47.3
13	0.06	7	20	55.6
14	0.06	7	20	50.9
15	0.06	7	20	52.4
16	0.06	7	20	51.5
17	0.06	7	20	57.1

RBBR removal efficiency of 90.9% was achieved in experimental run 2, where the CHI-BZI/OC/Fe₃O₄ dosage was 0.1 g/100 mL, pH was 4.0, and the contact time was 20 min. With ranges of beginning RBBR concentrations (20–120 mg/L) and contact times (0–360 min), these ideal circumstances were used for the analysis of adsorption isotherms and kinetic experiments. The equilibrium adsorption capacity of CHI-BZI/OC/Fe₃O₄ towards RBBR at equilibrium time was determined using Eq. (3).

$$q_e = \frac{(C_o - C_e)V}{W} \quad (3)$$

where the volume of RBBR solution is V (L) and the mass of CHI-BZI/OC/Fe₃O₄ is W (g).

3 Results and discussion

3.1 Characterization

The physicochemical properties of the CHI-BZI/OC/Fe₃O₄ are detailed in Table 3. The BET surface area of CHI-BZI/OC/Fe₃O₄ was 1.78 m²/g; whereas, the mean pore diameter was found to be 22.9 nm. According to the established IUPAC classification, this average pore diameter signifies that the structure of CHI-BZI/OC/Fe₃O₄ falls under the category of mesostructured materials [31]. Furthermore,

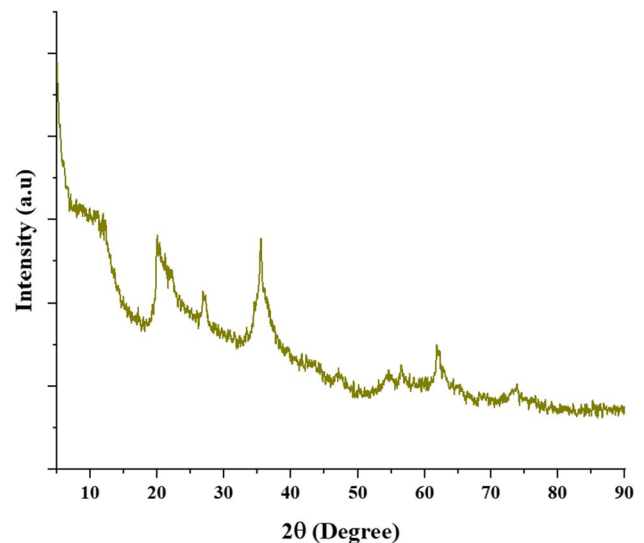
Table 3 Physiochemical characteristics of CHI-BZI/OC/Fe₃O₄

Parameter(s)	CHI-BZI/ OC/Fe ₃ O ₄
Surface area (m ² /g)	1.78
Langmuir surface area (m ² /g)	2.10
Pore volume (cm ³ /g)	0.0099
Pore diameter (nm)	22.9

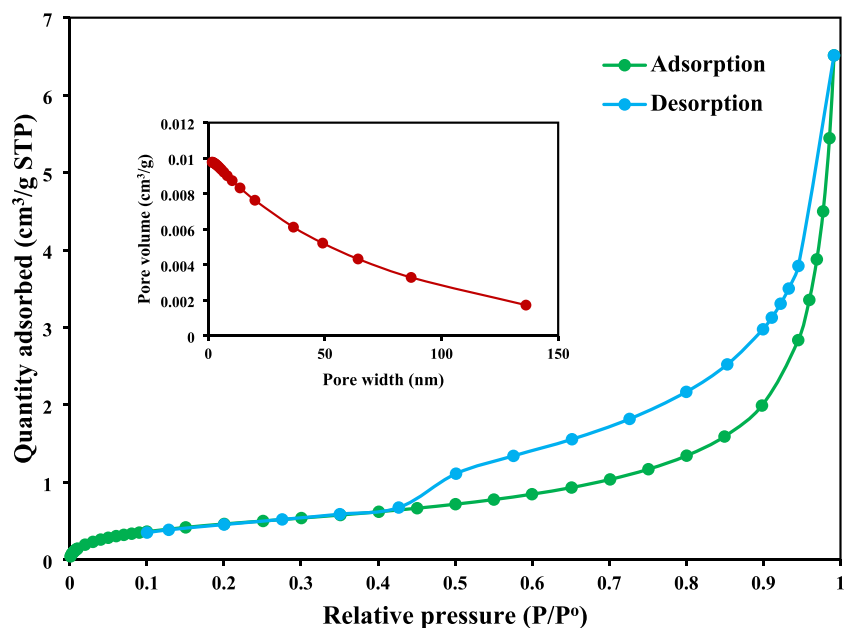
the nitrogen adsorption/desorption isotherms observed for CHI-BZI/OC/Fe₃O₄ exhibited a Type-IV isotherm pattern (see Fig. 1). The accompanying figure displayed within Fig. 1 visually depicts the correlation between pore volume and pore sizes. The Type-IV isotherm pattern and the corresponding plot provide substantial evidence that CHI-BZI/OC/Fe₃O₄ possesses a mesoporous structure that exists in a significant range of pore diameters [32].

XRD technique was applied to meticulously investigate the phase composition and crystalline property of the CHI-BZI/OC/Fe₃O₄. The XRD spectrum of this composite is visually represented in Fig. 2. The sharp peak located at $2\theta = 21^\circ$ is indicative of presence CHI [33]. XRD pattern of CHI-BZI/OC/Fe₃O₄ presents key peaks at $2\theta = 35.6^\circ$, 43° , 53° , 57.4° , and 62.4° providing clear evidence of the incorporation of Fe₃O₄ into the CHI-BZI/OC/Fe₃O₄ [34].

The FT-IR spectral analysis method was utilized to investigate the CHI-BZI/OC/Fe₃O₄'s synthesis and its interaction with RBBR. The results from the FT-IR data of CHI-BZI/OC/Fe₃O₄ and CHI-BZI/OC/Fe₃O₄-RBBR are illustrated in Fig. 3. The FT-IR spectrum of CHI-BZI/OC/Fe₃O₄ revealed major peaks (3500–3800 cm⁻¹) that signified the stretching

**Fig. 2** XRD pattern of CHI-BZI/OC/Fe₃O₄

vibration generated by the hydroxyl and amino groups [35]. There were also absorption peaks at 2900–2800 cm⁻¹, which were associated with the presence of chitosan-related C-H [36]. In addition, a peak at 1650 cm⁻¹ revealed a stretching vibration driven by the existence of the C=N bond as a result of the BZI grafting process in CHI chains [20]. Peaks at 1370 cm⁻¹ (C–N) and 1030 cm⁻¹ (C–O) could be assigned to the CHI [20]. The strong band detected at 1030 cm⁻¹ can also be attributed to the Si–O stretching vibration, while the Fe–O bonds were supported by a vibrational band at 570 cm⁻¹ [37, 38]. The FT-IR spectrum of CHI-BZI/OC/Fe₃O₄-RBBR resembled that of Fig. 3a, with some peaks'

Fig. 1 The N₂ adsorption–desorption isotherms and pore size distribution of CHI-BZI/OC/Fe₃O₄

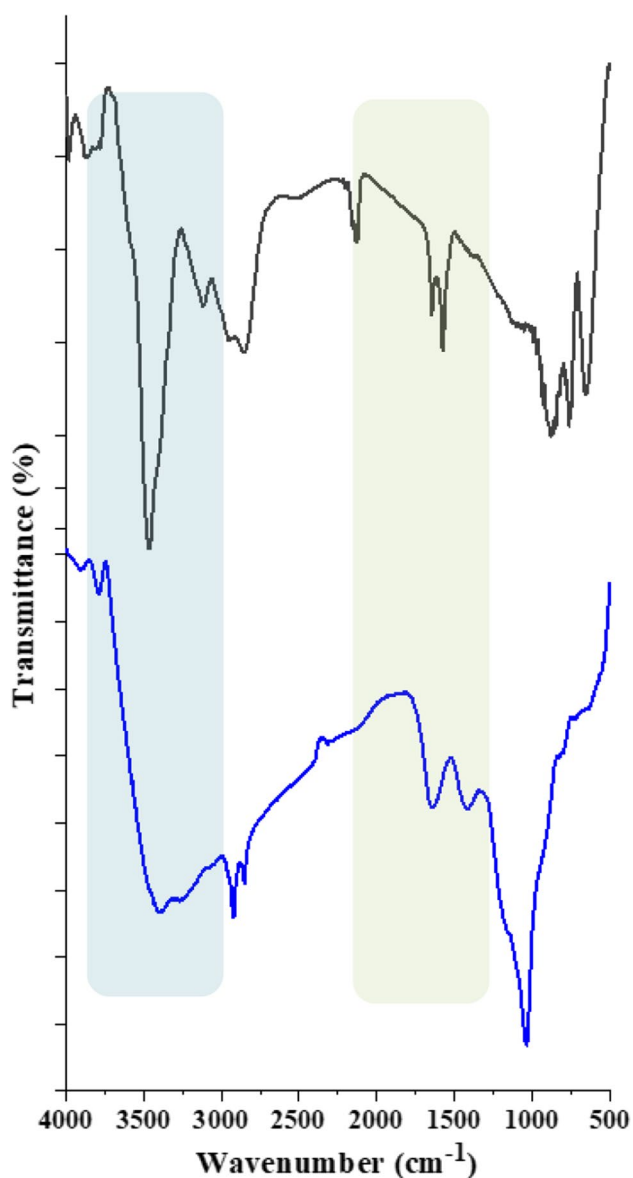


Fig. 3 FTIR spectra of (a) CHI-BZI/OC/Fe₃O₄ and (b) CHI-BZI/OC/Fe₃O₄ after RBBR adsorption

positions shifted, especially the OH and -NH₂ groups, indicating that RBBR had been adsorbed onto the CHI-BZI/OC/Fe₃O₄ surface.

The morphological characteristic of the adsorbent (CHI-BZI/OC/Fe₃O₄) before and after the uptake of the adsorbate (RBBR) was investigated using SEM–EDX analysis as shown in Fig. 4. The SEM image and EDX spectrum of the CHI-BZI/OC/Fe₃O₄ surface before RBBR adsorption are presented in Fig. 4a and 4b respectively. As can be seen from Fig. 4a, the surface of CHI-BZI/OC/Fe₃O₄ before adsorption appears as a wavy, irregular, and

heterogeneous surface. Moreover, its corresponding EDX spectrum (Fig. 4b) shows the presence of the Fe, C, Fe, N, S, O, and Si in its molecular structure, and the presence of Fe confirms the existence of Fe₃O₄ in the CHI-BZI/OC/Fe₃O₄ which is responsible for its magnetic property. On the other hand, the SEM image of CHI-BZI/OC/Fe₃O₄ after RBBR adsorption (Fig. 4c) presents a more compact surface and less heterogeneous surface which can be attributed to the loading of RBBR dye molecules onto CHI-BZI/OC/Fe₃O₄ surface. Additionally, the elemental composition of CHI-BZI/OC/Fe₃O₄ after RBBR adsorption (Fig. 4d) shows similar profile to elemental composition of CHI-BZI/OC/Fe₃O₄ before RBBR adsorption (Fig. 4b).

3.2 BBD Model Fitting

The RBBR removal data obtained from the experiments were analyzed using ANOVA. The statistical data are outlined in Table 4, and the model F-value of 95.06 indicates that the created model (RBBR removal) is significant from a statistical perspective [39]. The correlation coefficient (R²) value of 0.99 implies a good link between the real and theoretical RBBR removal values [40]. When the P-value is less than 0.05, model codes are considered significant terms. Therefore, AB, AC, BC, A, B, C, and C² were identified as important terms for removing RBBR. The quadratic polynomial model, as shown in Eq. (4), was applied to establish the actual link between RBBR removal and the factors.

$$\begin{aligned} \text{RBBR removal(\%)} = & +53.50 + 25.26A - 4.35B + 15.04C \\ & - 4.20AB + 6.88AC - 6.95BC - 12.81C^2 \end{aligned} \quad (4)$$

To verify the experimental data, the real versus theoretical plot and the normal probability plot of residuals extracted from the BBD model were analyzed. Figure 5a shows the real versus theoretical plot of RBBR removal (%), where the real points were found to be mostly close to the theoretical points, signifying the strength of the applied model. Figure 5b shows the normal probability plot of residuals, which indicates the independence of the residuals [41]. The residuals may be properly distributed, according to the normal distribution of all the points surrounding the straight line. Using Cook's distance, another statistical validation was carried out, as shown in Fig. 5c. Cook's distance should be less than 1 to be considered acceptable. All observed values in this investigation were less than 1, and the majority of runs were even lower than 0.2, showing significant implications for the model's predictive capacity [42]. The quality and dependability of the experimental results acquired from the BBD model are confirmed by these statistical validations.

Fig. 4 (a) and (b) SEM image and EDX spectrum of CHI-BZI/OC/Fe₃O₄ respectively; (c) and (d) SEM image and EDX spectrum of CHI-BZI/OC/Fe₃O₄ after RBBR adsorption respectively

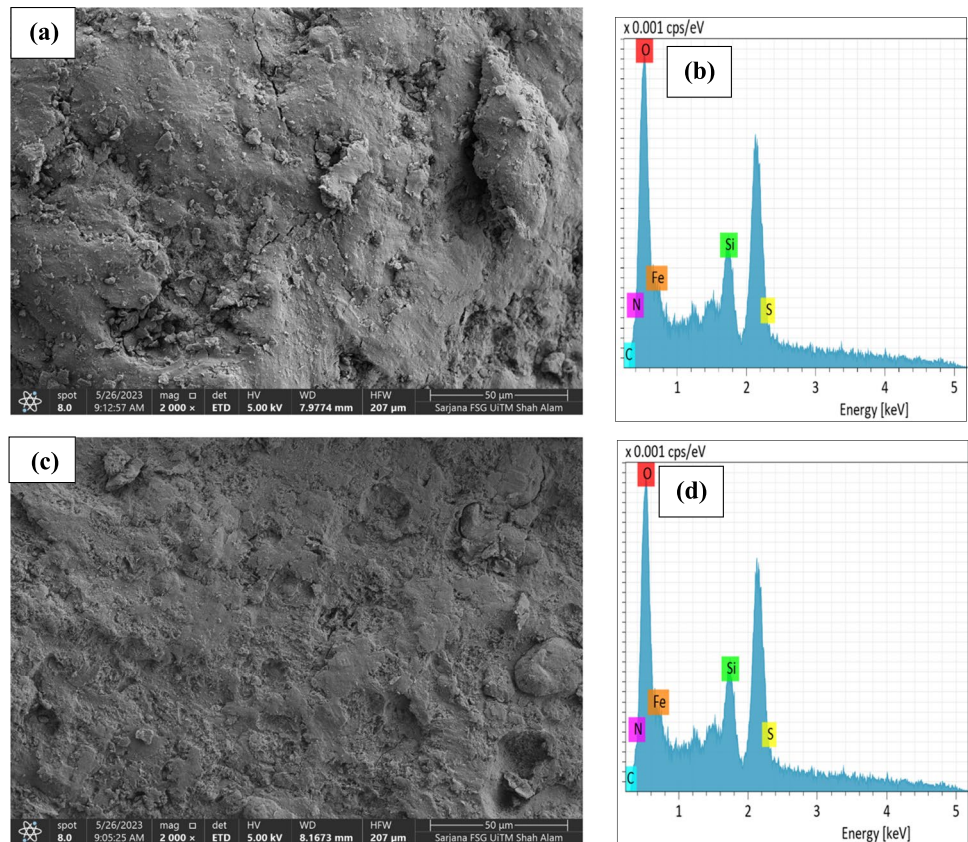


Table 4 ANOVA analysis for RBBR removal (%) by CHI-BZI/OC/Fe₃O₄

Source	Sum of Squares	df	Mean Square	F-value	p-value
Model	8212.56	9	912.51	95.06	<0.0001
A	5105.55	1	5105.55	531.89	<0.0001
B	151.38	1	151.38	15.77	0.0054
C	1809.01	1	1809.01	188.46	<0.0001
AB	70.56	1	70.56	7.35	0.0301
AC	189.06	1	189.06	19.70	0.0030
BC	193.21	1	193.21	20.13	0.0028
A ²	8.11	1	8.11	0.8445	0.3887
B ²	0.4112	1	0.4112	0.0428	0.8419
C ²	691.20	1	691.20	72.01	<0.0001
Residual	67.19	7	9.60		
Lack of Fit	37.85	3	12.62	1.72	0.3002
Pure Error	29.34	4	7.34		
Cor Total	8279.76	16			

3.3 Effects of Significant Interactions

Figure 6a-b showcases the 3D response surfaces and 2D contour plots, providing an insight into the dual impacts of parameters on RBBR removal (%). Specifically, the key interaction between CHI-BZI/OC/Fe₃O₄ dose and pH is

presented in these plots. Upon analysis, it becomes evident that the RBBR removal gradually increases with a decrease in solution pH, eventually reaching a pH of 4. This result is closely linked to the CHI-BZI/OC/Fe₃O₄'s surface charge, which was computed by the pH_{pzc} (cf. Fig. S2). The pH_{pzc} value, established as 6.9 for CHI-BZI/OC/Fe₃O₄, dictates that the biocomposite surface carries a negative charge when the pH is higher than 6.9, and conversely, a positive charge when the pH falls below 6.9. As the solution pH decreases, creating a more acidic environment, the -NH₂ groups on the surface of the CHI-BZI/OC/Fe₃O₄ undergo protonation due to the presence of H⁺ ions. Consequently, this protonation leads to a positive charge on the biocomposite surface. The outcome of this charge variation is an electrostatic force between the cationic sites on the CHI-BZI/OC/Fe₃O₄ surface and the RBBR, as outlined in Eq. (5).

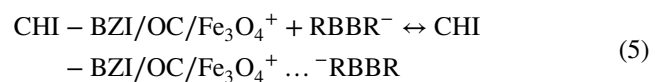
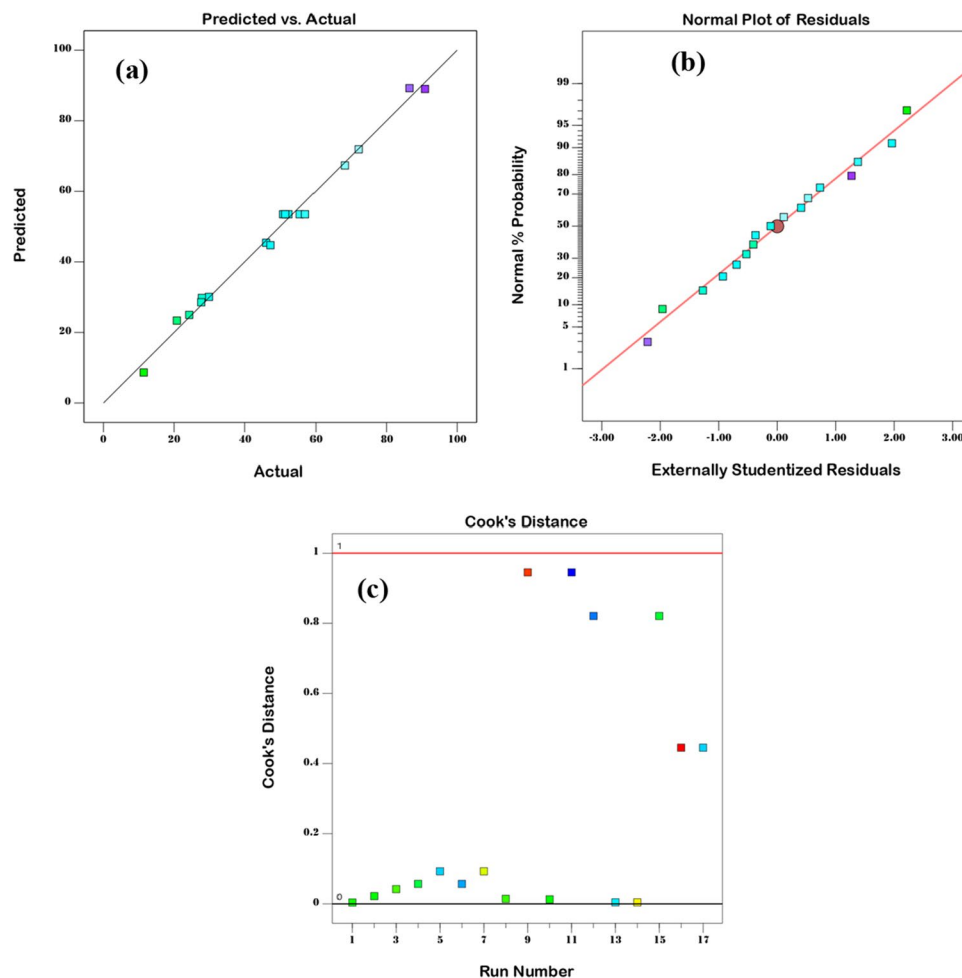


Figure 6a-b shows also increasing the adsorbent dose also contributes to higher RBBR removal. With higher doses of the CHI-BZI/OC/Fe₃O₄, more adsorption sites become available, increasing the overall adsorption capacity. This means that more RBBR dye molecules can interact with the active

Fig. 5 (a) plot of the relationship between the predicted and actual values; (b) normal probability plot of residuals; (c) Cook's distance plot for RBBR adsorption by CHI-BZI/OC/Fe₃O₄



sites on the adsorbent surface, resulting in a higher percentage of dye removal. The combination of lower pH and higher adsorbent dose creates a synergistic effect, further enhancing the adsorption of RBBR. The positive charge on the adsorbent's surface is intensified at lower pH, increasing the attraction to the negatively charged dye molecules. The analysis of Fig. 6c-f reveals significant interactions between AC (dose \times time) and BC (pH \times time) in the adsorption of RBBR using the CHI-BZI/OC/Fe₃O₄. These interactions indicate that both contact time and the combination of adsorbent dose and pH have a substantial impact on RBBR removal (%). The results in Fig. 6c-f show that the removal of RBBR (%) increases rapidly as the contact time is extended from 5 to 35 min. This observation can be explained by considering that more contact time allows RBBR dye molecules sufficient time to diffuse and penetrate into the CHI-BZI/OC/Fe₃O₄'s pores.

3.4 Adsorption Study

This study was performed to investigate the effect of contact time and initial RBBR concentrations on the adsorption capacity of CHI-BZI/OC/Fe₃O₄. During the experiments, the

CHI-BZI/OC/Fe₃O₄ dose (0.1), pH (4.0), and temperature (25 °C) were held constant. The results, as depicted in Fig. 7a, obviously show that the adsorption ability of the CHI-BZI/OC/Fe₃O₄ material for RBBR uptake increased rapidly (from 17.2 to 96.1) initially and then reached a plateau for all studied initial RBBR concentrations. The large increase in adsorption capacity at the beginning can be attributed to the high availability of the specific surface area of the adsorbent active sites of CHI-BZI/OC/Fe₃O₄. As the contact time increased, more RBBR molecules were able to interact with the adsorbent, leading to higher uptake. However, beyond a certain contact time, the adsorption capacity plateaued, indicating that the adsorption sites on the CHI-BZI/OC/Fe₃O₄ surface were saturated, and no further adsorption occurred. This plateau suggests that the maximum adsorption capacity of the CHI-BZI/OC/Fe₃O₄ material for RBBR has been reached under the given experimental conditions. Furthermore, an interesting observation is that the initial RBBR concentration in the solution also influences the adsorption capacity. As the initial concentration of RBBR increased, the driving force for adsorption also increased, resulting in more RBBR molecules being adsorbed by the CHI-BZI/OC/Fe₃O₄ [43].

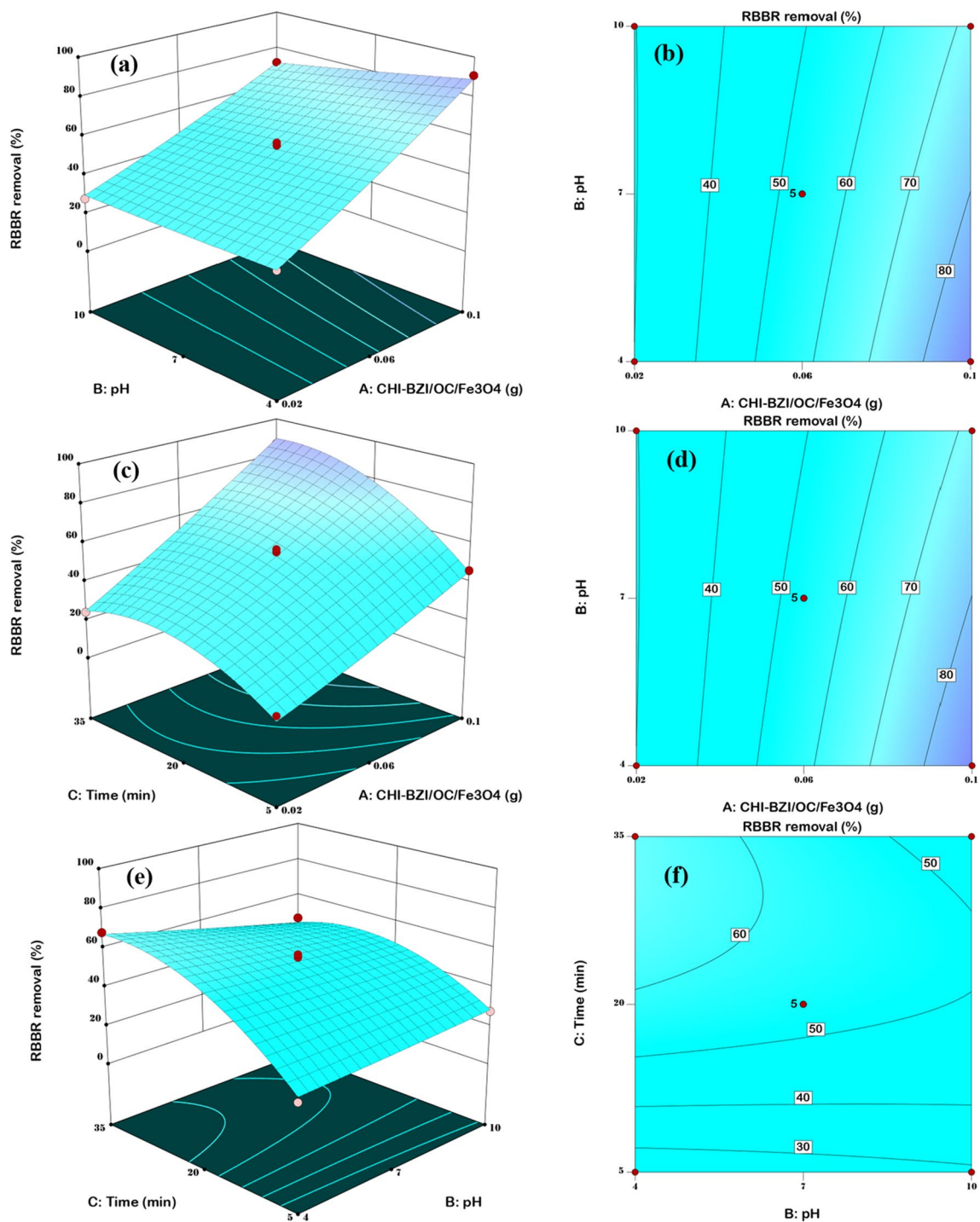


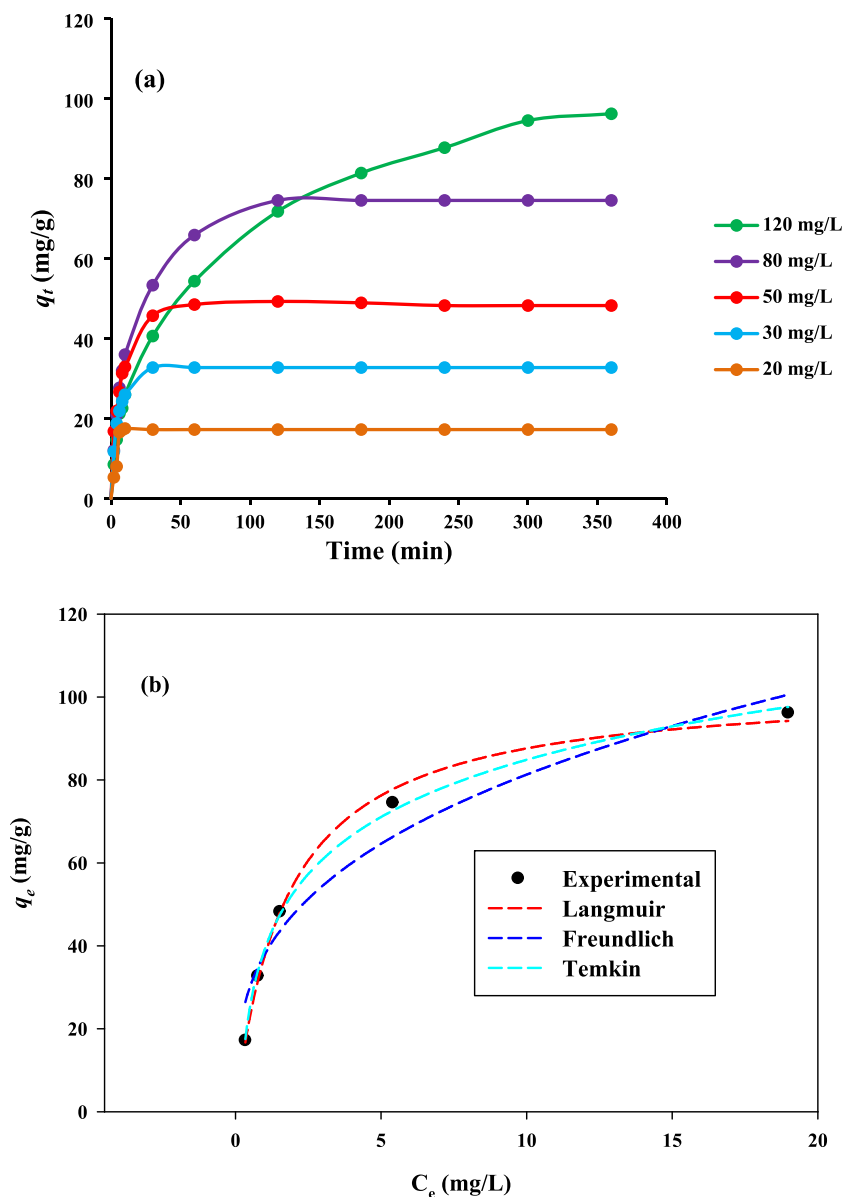
Fig. 6: 3D and 2D plots AB (a: 3D; b: 2D), AC (c: 3D; d: 2D), and BC (e: 3D; f: 2D) interactions

3.5 Adsorption Kinetic

The adsorption kinetics provides valuable information about how quickly the adsorption process occurs and gain insights into the mechanism of the adsorption process. The kinetics of RBBR adsorption using the CHI-BZI/OC/Fe₃O₄ were

analyzed by employing the pseudo-second order (PSO) kinetic [44] and pseudo-first order (PFO) kinetic [45] as provided in Table S1. Table 5 presents the kinetic findings for the PFO and PSO models. The outcomes indicate that the RBBR adsorption onto the CHI-BZI/OC/Fe₃O₄ was governed by PSO kinetic model as confirmed by comapable

Fig. 7 (a) Effect of the contact time on RBBR adsorption by CHI-BZI/OC/Fe₃O₄ at several concentrations and (b) adsorption isotherms (dose=0.1 g/100 mL, and pH=4)



values of the theoretical q_e and experimental q_e values. Thus, further confirmation was made by using root means square error (RMSE) the sum of squares error (SSE) in Table 5. In fact, the low values of the RMSE and SSE for

PSO over PFO indicate the best fit for the PSO to the experimental data, and revealing that both chemisorption and physisorption modes played a crucial role in the interaction between the CHI-BZI/OC/Fe₃O₄ and RBBR [46].

Table 5 PFO and PSO Kinetics parameters for RBBR adsorption on CHI-BZI/OC/Fe₃O₄

Concentration (mg/L)	$q_{e\text{ exp}}$ (mg/g)	PFO					PSO				
		$q_{e\text{ cal}}$ (mg/g)	k_1 (1/min)	R^2	SSE	RMSE	$q_{e\text{ cal}}$ (mg/g)	$k_2 \times 10^{-2}$ (g/mg min)	R^2	SSE	RMSE
20	17.2	17.5	0.253	0.93	27.3	1.45	18.1	2.409	0.86	53.9	2.04
30	32.7	32.6	0.188	0.99	8.68	0.82	33.7	0.921	0.99	8.77	0.82
50	48.2	48.1	0.137	0.98	44.4	1.85	50.2	0.415	0.99	22.5	1.32
80	74.5	72.5	0.066	0.98	178.9	3.72	78.2	0.110	0.99	25.1	1.39
120	96.1	88.9	0.019	0.95	651.9	7.08	101.7	0.025	0.98	287.9	4.71

Table 6 The parameters of isotherm models and equilibrium parameters for RBBR adsorption on CHI-BZI/OC/Fe₃O₄

Adsorption isotherm	Parameter	Value
Langmuir	q_m (mg/g)	102.9
	K_L (L/mg)	0.57
	R^2	0.99
	SSE	16.6
	RMSE	1.82
Freundlich	K_F (mg/g) (L/mg) ^{1/n}	37.8
	n	3.01
	R^2	0.95
	SSE	198.1
	RMSE	6.29
Temkin	K_T (L/mg)	1.96
	b_T (J/mol)	124.5
	R^2	0.99
	SSE	7.23
	RMSE	1.21

3.6 Adsorption Isotherm

The adsorption isotherm analysis provides valuable insights into the adsorption behavior of RBBR on CHI-BZI/OC/Fe₃O₄ and confirms its outstanding performance as an adsorbent for the removal of this dye from wastewater. To analyze the adsorption equilibrium data, three isotherm models i.e., Langmuir [47], Freundlich [48], and Temkin [49] were used. Table S1 contains a collection of the non-linear formulas for isotherms. Figure 7b shows the outcomes of the isotherms of RBBR adsorption. Based on the R^2 values shown in Table 6, the data from the adsorption equilibrium were considered to have the best fit. The results revealed that in comparison to the Freundlich isotherm ($R^2 = 0.95$), the Langmuir and Temkin models ($R^2 = 0.99$) gave a superior match to the equilibrium adsorption data of the batch experiment. As a result, the homogenous distribution of surface-active sites on the adsorbent surface allowed the Langmuir and Temkin isotherms to accurately estimate the adsorption of RBBR dye onto chitosan composite [50]. Hence, further confirmation for the suitability of the adsorption isotherm was made by using root means square error (RMSE) the sum of squares

error (SSE) as recorded in Table 6. In fact, the low values of the RMSE and SSE for the Langmuir isotherm model over Temkin and Freundlich isotherm models indicate a monolayer and homogeneous adsorption process of RBBR was occurred on the surface of CHI-BZI/OC/Fe₃O₄. Thus, the highest monolayer adsorption capacity calculated using the Langmuir model was 102.9 mg/g, which is greater than the values noted for most adsorbents (see Table 7).

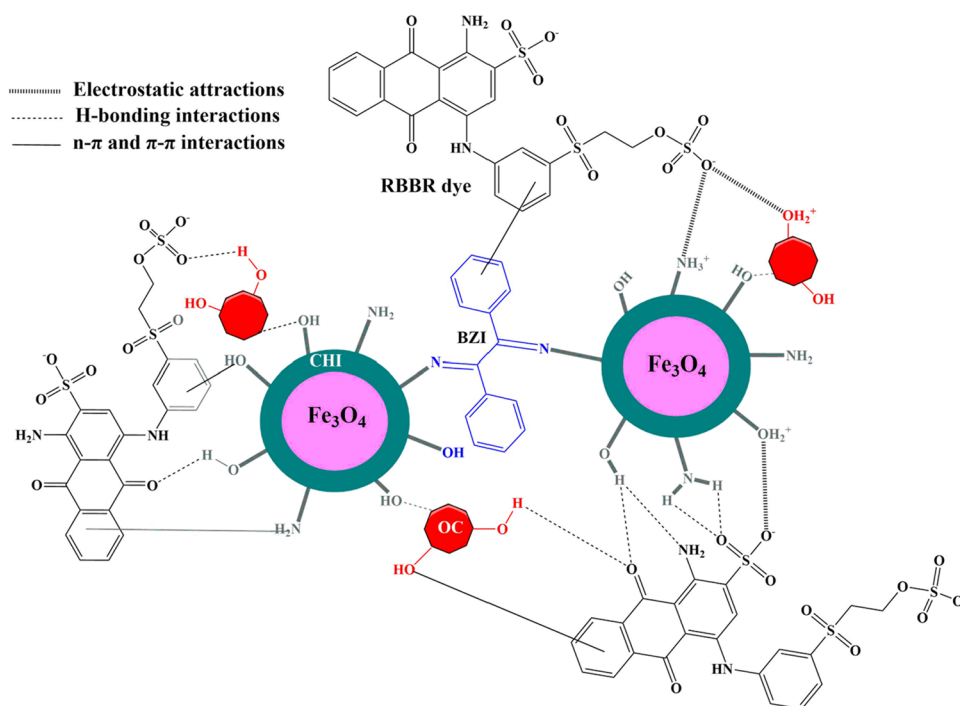
3.7 Adsorption Mechanism

Typically, chemisorption agrees with the Langmuir model, where monolayer formation indicates the chemical interactions between acidic RBBR dye molecules and CHI-BZI/OC/Fe₃O₄ adsorbent. These chemical interactions, facilitated by functional groups present on the surface of the CHI-BZI/OC/Fe₃O₄ adsorbent, play a fundamental role in the adsorption process, contributing to the overall effectiveness of the adsorption technique. The interaction of different functional groups present on the biocomposite surface plays a role in the adsorption process of RBBR on the surface of the CHI-BZI/OC/Fe₃O₄. These interactions are shown in Fig. 8, which further emphasizes the significant contribution of particular active groups to the adsorption of the RBBR dye. The positively charged protonated amino groups (-NH₃⁺), hydroxyl groups (-OH₂⁺), and silanol groups (SiOH₂⁺) are present in the CHI-BZI/OC/Fe₃O₄. The negatively charged sulfate groups (-SO₃⁻) of the RBBR dye are effectively attracted to and interacted with by these functional groups, causing the dye to bind to the surface of the biocomposite [48]. The adsorption process also heavily relies on interactions between hydrogen bonds. The nitrogen and oxygen atoms of the RBBR dye molecules create hydrogen bonds with the hydrogen atoms in the CHI-BZI/OC/Fe₃O₄. These hydrogen bonds improve the link between the dye and the biocomposite and increase its overall capacity for adsorption. The non-polar parts (e.g., -CH₂- groups) of the RBBR dye molecules can form hydrophobic interactions with the non-polar parts of the CHI-BZI/OC/Fe₃O₄ chains (e.g., -CH₂- groups). Additionally, π - π interactions between the

Table 7 Comparison of the adsorption capacity of CHI-BZI/OC/Fe₃O₄ with several adsorbents

Adsorbents	q_{max} (mg/g)	References
CHI-BZI/OC/Fe ₃ O ₄	102.9	This study
Chitosan/sepiolite clay/algae biocomposite	292.4	[51]
ZnO-polyacrylonitrile-hinokitiol	267.37	[52]
Chitosan-alkali lignin composite	111.11	[53]
Powder Activated Carbon/Maghemite composite	105.5	[54]
Chitosan/SiO ₂ /carbon nanotubes magnetic nanocomposite	97.08	[55]
Mesoporous Fe-Al-doped cellulose	95.62	[56]
Modified-KSF-montmorillonite	38.99	[57]
Borax cross-linked Jhingan gum hydrogel	9.884	[58]

Fig. 8 Illustration of the possible interaction between CHI-BZI/OC/Fe₃O₄ and RBBR including electrostatic forces, hydrogen bonding, π - π , and n- π interactions



π system in the RBBR and the electron donor system in the CHI-BZI/OC/Fe₃O₄ play a key role in the adsorption. A crucial part of the adsorption process is also played by the BZI aromatic ring, which is grafted onto the polymeric matrix of CHI-BZI/OC/Fe₃O₄. The RBBR dye molecules are strongly adsorbed due to interactions between the BZI ring grafted on the biocomposite and the aromatic rings in the dye. In conclusion, the CHI-BZI/OC/Fe₃O₄ presents itself as a very effective adsorbent for the removal of RBBR from aqueous solutions due to the combination of these many interactions, including protonated amino groups, π - π interactions, hydrogen bonding, and n- π .

4 Conclusions

CHI-BZI/OC/Fe₃O₄ was successfully synthesized as a bioadsorbent for the removal of RBBR from the aquatic system. The experimental results of the BBD model illustrated that the highest RBBR removal of 90.9% was achieved at a CHI-BZI/OC/Fe₃O₄ dosage of 0.1 g/100 mL, pH of 4.0, and time of 20 min. Both isotherm models namely Langmuir and Temkin provided a good fit to the experimental data, indicating that the adsorption process occurs on a single layer of adsorbate molecules on the CHI-BZI/OC/Fe₃O₄ surface, and the heat of adsorption decreases linearly with coverage. The experimental data indicated that the uptake of RBBR by CHI-BZI/OC/Fe₃O₄ is governed by chemisorption process. The q_{max} of CHI-BZI/OC/Fe₃O₄ for RBBR was determined

to be 102.9 mg/g. The mechanics of RBBR adsorption by CHI-BZI/OC/Fe₃O₄ include electrostatic forces, π - π , hydrogen bonding, and n- π interactions. These insights gleaned from the present work provide valuable information for the potential applications of this biocomposite material in wastewater treatment and environmental remediation efforts.

Supplementary Information The online version contains supplementary material available at <https://doi.org/10.1007/s10904-024-03120-5>.

Acknowledgements The authors are thankful to the Faculty of Applied Sciences, Universiti Teknologi MARA (UiTM) Shah Alam, Malaysia for the research facilities. The author Ahmad Hapiz is thankful to the Government of West Nusa Tenggara (NTB) Province, Indonesia, as well as the Education Development Institute (LPP) NTB and the Regional Research and Innovation Agency (BRIDA) NTB for providing a fully funded scholarship. The author (Ruihong Wu) would like to thank Hengshui University for its scientific research funding (2023ZRZ01). The author (Zeid A. ALOthman) is grateful to the Researchers Supporting Project No. (RSP2024R1), King Saud University, Riyadh, Saudi Arabia.

Authors Contributions All authors contributed to the study conception and design. Material preparation, data collection and analysis were performed by Ali H. Jawad, Ahmed Saud Abdulhameed, Ahmad Hapiz, Salis Awal Musa, Ruihong Wu, and Zeid A. ALOthman. The first draft of the manuscript was written by Ahmed Saud Abdulhameed, Ahmad Hapiz, Ali H. Jawad, and all authors commented on previous versions of the manuscript. All authors read and approved the final manuscript.

Funding The author (Ruihong Wu) would like to thank Hengshui University for its scientific research funding (2023ZRZ01). The author (Zeid A. ALOthman) is thankful to the Researchers Supporting Project No. (RSP2024R1), King Saud University, Riyadh, Saudi Arabia.

Data Availability The datasets used and/or analyzed during the current study are available from the corresponding author on reasonable request.

Declarations

Ethical Approval Not applicable.

Consent to Participate Not applicable.

Consent to Publish Not applicable.

Competing Interests The authors declare that they have no competing interests.

References

- M.E. Mahmoud, A.M. El-Ghanam, S.R. Saad, Fast and efficient adsorptive capture of Congo red and Erythromycin pollutants by a novel nanobiosorbent from crosslinked nanosilica with nanobiochar and chitosan. *Inorg. Chem. Commun.* **158**, 111557 (2023)
- A.M. Hameed, Synthesis of Si/Cu Amorphous Adsorbent for Efficient Removal of Methylene Blue Dye from Aqueous Media. *J. Inorg. Organomet. Polym.* **30**(8), 2881–2889 (2020)
- R. Al-Tohamy, S.S. Ali, F. Li, K.M. Okasha, Y.A.G. Mahmoud, T. Elsamahy, J. Sun, A critical review on the treatment of dye-containing wastewater: Ecotoxicological and health concerns of textile dyes and possible remediation approaches for environmental safety. *Ecotoxicol. Environ. Saf.* **231**, 113160 (2022)
- A. Kalra, A. Gupta, Recent advances in decolorization of dyes using iron nanoparticles: A mini review. *Mater. Today: Proc.* **36**, 689–696 (2021)
- A. Shahinpour, B. Tanhaei, A. Ayati, H. Beiki, M. Sillanpää, Binary dyes adsorption onto novel designed magnetic clay-biopolymer hydrogel involves characterization and adsorption performance: Kinetic, equilibrium, thermodynamic, and adsorption mechanism. *J. Mol. Liq.* **366**, 120303 (2022)
- A. Belcaid, B.H. Beakou, S. Bouhsina, A. Anouar, Insight into adsorptive removal of methylene blue, malachite green, and rhodamine B dyes by cassava peel biochar (*Manihot esculenta Crantz*) in single, binary, and ternary systems: competitive adsorption study and theoretical calculations. *Biomass Convers. Biorefin.* **14**, 7783–7806 (2022)
- J. Hou, K. Wang, R. Weng, L. Li, Y. Liu, J. Sheng, Y. Song, Purification of dye-contaminated water using Si-doped mesoporous Fe₃O₄ prepared with rice husk SBA-15 as a template: behavior and mechanism. *Biomass Convers. Biorefin.* **14**, 985–999 (2022)
- C. Lu, J. Yang, A. Khan, J. Yang, Q. Li, G. Wang, A highly efficient technique to simultaneously remove acidic and basic dyes using magnetic ion-exchange microbeads. *J. Environ. Manage.* **304**, 114173 (2022)
- T. Pei, M. Deng, C. Ma, H. Yan, A. Zhu, L. Ye, Q. Zhang, Loose nanofiltration membranes based on interfacial glutaraldehyde-amine polymerization for fast and highly selective dye/salt separation. *Chem. Eng. J.* **450**, 138057 (2022)
- M. Ikram, M. Naeem, M. Zahoor, M.M. Hanafiah, A.A. Oyekanmi, R. Ullah, N. Gulfam, Biological degradation of the azo dye basic orange 2 by *Escherichia coli*: A sustainable and ecofriendly approach for the treatment of textile wastewater. *Water* **14**(13), 2063 (2022)
- J. Kalita, B. Das, S.S. Dhar, Synergistic effect of iron and copper in hydroxyapatite nanorods for Fenton-like oxidation of organic dye. *Colloids Surf A Physicochem Eng Asp* **643**, 128750 (2022)
- U. Ewuzie, O.D. Saliu, K. Dulta, S. Ogunniyi, A.O. Bajeh, K.O. Iwuozor, J.O. Ighalo, A review on treatment technologies for printing and dyeing wastewater (PDW). *J. Water Process Eng.* **50**, 103273 (2022)
- S. Afzal, S. Hassan, Z. Imran, S. Aminullah. Chitosan Based Polymer Membrane Modified with CuO/Graphene Oxide Nanoparticles: Novel Synthesis, Characterization and Enhanced Methyl Orange Removal. *J. Inorg. Organomet. Polym.* (2024). <https://doi.org/10.1007/s10904-024-03008-4>
- H. Zhu, S. Chen, H. Duan, J. He, Y. Luo, Removal of anionic and cationic dyes using porous chitosan/carboxymethyl cellulose-PEG hydrogels: Optimization, adsorption kinetics, isotherm and thermodynamics studies. *Int. J. Biol. Macromol.* **231**, 123213 (2023)
- M.E. El-Naggar, E.K. Radwan, H.R. Rashdan, S.T. El-Wakeel, A.A. Koryam, A. Sabt, Simultaneous removal of Pb²⁺ and direct red 31 dye from contaminated water using N-(2-hydroxyethyl)-2-oxo-2 H-chromene-3-carboxamide loaded chitosan nanoparticles. *RSC Adv.* **12**(29), 18923–18935 (2022)
- A.S. Abdulhameed, A.H. Jawad, M. Ridwan, T. Khadiran, L.D. Wilson, Z.M. Yaseen, Chitosan/carbon-doped TiO₂ composite for adsorption of two anionic dyes in solution and gaseous SO₂ capture: experimental modeling and optimization. *J. Polym. Environ.* **30**(11), 4619–4636 (2022)
- A. Benettayeb, S. Ghosh, M. Usman, F.Z. Seihoub, I. Sohoo, C.H. Chia, M. Sillanpää, Some well-known alginate and chitosan modifications used in adsorption: A review. *Water* **14**(9), 1353 (2022)
- M. Keshvardoostchokami, M. Majidi, A. Zamani, B. Liu, A review on the use of chitosan and chitosan derivatives as the bio-adsorbents for the water treatment: Removal of nitrogen-containing pollutants. *Carbohydr. Polym.* **273**, 118625 (2021)
- U. Filipkowska, T. Józwiak, Application of chemically-cross-linked chitosan for the removal of Reactive Black 5 and Reactive Yellow 84 dyes from aqueous solutions. *J. Polym. Eng.* **33**(8), 735–747 (2013)
- N. I. Normi, A. S. Abdulhameed, S. N. Surip, Z. A. ALOthman, L. D. Wilson, A. H. Jawad. Benzil Schiff Base Side-Chain Polymer-Crosslinked Chitosan Via Hydrothermal Process for Reactive Orange 16 Dye Removal: An Optimized and Comparative Study with Chitosan. *J. Polym. Environ.* **31**(5) (2023) 1986–2004.
- E. M. Abd El-Monaem, A. S. Eltaweil, H. M. Elshishini, M. Hosny, M. M. Abou Alsoaud, N. F. Attia, A. M. Omer. Sustainable adsorptive removal of antibiotic residues by chitosan composites: An insight into current developments and future recommendations. *Arab. J. Chem.* **15**(5) (2022) 103743.
- X.Q. Liu, X.X. Zhao, Y. Liu, T.A. Zhang, Review on preparation and adsorption properties of chitosan and chitosan composites. *Polym. Bull.* **79**(4), 2633–2665 (2022)
- S. Pandey, S.B. Mishra, Organic–inorganic hybrid of chitosan/organoclay bionanocomposites for hexavalent chromium uptake. *J. Colloid Interface Sci.* **361**(2), 509–520 (2011)
- S. Mao, M. Gao, Functional organoclays for removal of heavy metal ions from water: A review. *J. Mol. Liquids* **334**, 116143 (2021)
- T. Shen, M. Gao, Gemini surfactant modified organo-clays for removal of organic pollutants from water: A review. *Chem. Eng. J.* **375**, 121910 (2019)
- T. De Oliveira, M. Boussafir, L. Fougère, E. Destandau, Y. Sugahara, R. Guégan, Use of a clay mineral and its nonionic and cationic organoclay derivatives for the removal of pharmaceuticals from rural wastewater effluents. *Chemosphere* **259**, 127480 (2020)
- M.B. de Farias, M.P. Spaolonzi, M.G.C. Silva, M.G.A. Vieira, Fixed-bed adsorption of bisphenol A onto organoclay: Characterization, mathematical modelling and theoretical calculation of DFT-based chemical descriptors. *J. Environ. Chem. Eng.* **9**(5), 106103 (2021)

28. K. Fang, L. Deng, J. Yin, T. Yang, J. Li, W. He, Recent advances in starch-based magnetic adsorbents for the removal of contaminants from wastewater: A review. *Int. J. Biol. Macromol.* **218**, 909–929 (2022)
29. G.D.V. Brião, J.R. de Andrade, M.G.C. da Silva, M.G.A. Vieira, Removal of toxic metals from water using chitosan-based magnetic adsorbents. A review. *Environ. Chem. Lett.* **18**, 1145–1168 (2020)
30. A.R. Sedaghatian, A. Marjani, A.H. Joshaghani, R. Mohammad-Rezaei, Synthesis of magnetic graphene quantum dots–chitosan nanocomposite: an efficient adsorbent for removal of Pb²⁺ from aqueous solution. *Int. J. Environ. Sci. Technol.* **19**(11), 11447–11458 (2022)
31. K.S. Sing, Reporting physisorption data for gas/solid systems with special reference to the determination of surface area and porosity (Recommendations 1984). *Pure Appl. Chem.* **57**(4), 603–619 (1985)
32. S. Korde, S. Tandekar, R.M. Jugade, Novel mesoporous chitosan-zirconia-ferrosioferic oxide as magnetic composite for defluoridation of water. *J. Environ. Chem. Eng.* **8**(5), 104360 (2020)
33. K. Ssekatawa, D.K. Byarugaba, E.M. Wampande, T.N. Moja, E. Nxumalo, M. Maaza, J.B. Kirabira, Isolation and characterization of chitosan from Ugandan edible mushrooms. Nile perch scales and banana weevils for biomedical applications. *Sci. Rep.* **11**(1), 4116 (2021)
34. M.A. Hefnawy, S.S. Medany, R.M. El-Sherif, S.A. Fadlallah, Green synthesis of NiO/Fe₃O₄@ chitosan composite catalyst based on graphite for urea electro-oxidation. *Mater. Chem. Phys.* **290**, 126603 (2022)
35. S. Barkhordari, A. Alizadeh, M. Yadollahi, H. Namazi, One-pot synthesis of magnetic chitosan/iron oxide bio-nanocomposite hydrogel beads as drug delivery systems. *Soft Mater.* **19**(4), 373–381 (2021)
36. Z.M. Şenol, N. Gürsoy, S. Şimşek, A. Özer, N. Karakuş, Removal of food dyes from aqueous solution by chitosan-vermiculite beads. *Int. J. Biol. Macromol.* **148**, 635–646 (2020)
37. U. Malayoglu, Removal of heavy metals by biopolymer (chitosan)/nanoclay composites. *Sep. Sci. Technol.* **53**(17), 2741–2749 (2018)
38. E. Asgari, A. Sheikhmohammadi, J. Yeganeh, Application of the Fe₃O₄-chitosan nano-adsorbent for the adsorption of metronidazole from wastewater: Optimization, kinetic, thermodynamic and equilibrium studies. *Int. J. Biol. Macromol.* **164**, 694–706 (2020)
39. T. Thomas, A.K. Thalla, Nutmeg seed shell biochar as an effective adsorbent for removal of remazol brilliant blue reactive dye: kinetic, isotherm, and thermodynamic study. *Energy Sources, Part A: Recovery, Utilization, and Environmental Effects* **44**(1), 893–911 (2022)
40. Z. Alhalili, Green synthesis of copper oxide nanoparticles CuO NPs from Eucalyptus Globoulus leaf extract: Adsorption and design of experiments. *Arab. J. Chem.* **15**(5), 103739 (2022)
41. B.F. Shahandashty, N. Fallah, B. Nasernejad, Industrial wastewater treatment: Case study on copper removal from colloidal liquid using coagulation. *J. Water Process Eng.* **53**, 103712 (2023)
42. A.H. Jawad, B.H. Hameed, A.S. Abdulhameed, Synthesis of bio-hybrid magnetic chitosan-polyvinyl alcohol/MgO nanocomposite blend for remazol brilliant blue R dye adsorption: Solo and collective parametric optimization. *Polym. Bull.* **80**(5), 4927–4947 (2023)
43. Y. Ji, W. Zhang, H. Yang, F. Ma, F. Xu, Green synthesis of poly (pyrrole methane) for enhanced adsorption of anionic and cationic dyes from aqueous solution. *J. Colloid Interface Sci.* **590**, 396–406 (2021)
44. S. Lagergren, Zur theorie der sogenannten adsorption geloster stoffe. *Vet. Akad. Handl.* **24**, 1–39 (1898)
45. Y.S. Ho, G. McKay, Sorption of dye from aqueous solution by peat. *Chem. Eng. J.* **70**, 115–124 (1998)
46. P.S. Pauletto, J.O. Gonçalves, L.A.A. Pinto, G.L. Dotto, N.P.G. Salau, Single and competitive dye adsorption onto chitosan-based hybrid hydrogels using artificial neural network modeling. *J. Colloid Interface Sci.* **560**, 722–729 (2020)
47. I. Langmuir, The adsorption of gases on plane surfaces of glass, mica and platinum. *J. Am. Chem. Soc.* **40**, 1361–1403 (1918)
48. H.M.F. Freundlich, Over the adsorption in solution. *J. Phys. Chem.* **57**, 385–471 (1906)
49. M.I. Temkin, Kinetics of ammonia synthesis on promoted iron catalysts. *Acta Physiochim. URSS.* **12**, 327–356 (1940)
50. S. Pai, M.S. Kini, G. Rangasamy, R. Selvaraj, Mesoporous calcium hydroxide nanoparticle synthesis from waste bivalve clamshells and evaluation of its adsorptive potential for the removal of Acid Blue 113 dye. *Chemosphere* **313**, 137476 (2022)
51. Z. M. Zain, A. S. Abdulhameed, A. H. Jawad, Z. A. AlOthman, Z. M. Yaseen. A pH-sensitive surface of chitosan/sepiolite clay/algae biocomposite for the removal of malachite green and remazol brilliant blue R dyes: Optimization and adsorption mechanism study. *J. Polym. Environ.* **31**(2) (2023) 501–518.
52. D.N. Phan, R.A. Rebia, Y. Saito, D. Kharaghani, M. Khatri, T. Tanaka, I.S. Kim, Zinc oxide nanoparticles attached to polyacrylonitrile nanofibers with hinokitiol as gluing agent for synergistic antibacterial activities and effective dye removal. *J. Ind. Eng. Chem.* **85**, 258–268 (2020)
53. V. Nair, A. Panigrahy, R. Vinu, Development of novel chitosan–lignin composites for adsorption of dyes and metal ions from wastewater. *Chem. Eng. J.* **254**, 491–502 (2014)
54. B. Balci, F.E. Erkurt, M. Basibuyuk, F. Budak, Z. Zaimoglu, E.S. Turan, S. Yilmaz, Removal of Reactive Blue 19 from simulated textile wastewater by Powdered Activated Carbon/Maghemite composite. *Sep. Sci. Technol.* **57**(9), 1408–1426 (2022)
55. M. Abbasi, Synthesis and characterization of magnetic nanocomposite of chitosan/ SiO₂/carbon nanotubes and its application for dyes removal. *J. Clean. Prod.* **145**, 105–113 (2017)
56. M. Khapre, A. Shekhawat, D. Saravanan, S. Pandey, R. Jugade, Mesoporous Fe–Al-doped cellulose for the efficient removal of reactive dyes. *Mater. Adv.* **3**(7), 3278–3285 (2022)
57. M. M. Silva, M. M. Oliveira, M. C. Avelino, M. G. Fonseca, R. K. Almeida, E. C. Silva Filho. Adsorption of an industrial anionic dye by modified-KSF-montmorillonite: evaluation of the kinetic, thermodynamic and equilibrium data. *Chem. Eng. J.* **203** (2012) 259–268.
58. C.J. Mate, S. Mishra, Synthesis of borax cross-linked Jhingan gum hydrogel for remediation of Remazol Brilliant Blue R (RBBR) dye from water: adsorption isotherm, kinetic, thermodynamic and biodegradation studies. *Int. J. Biol. Macromol.* **151**, 677–690 (2020)

Publisher's Note Springer Nature remains neutral with regard to jurisdictional claims in published maps and institutional affiliations.

Springer Nature or its licensor (e.g. a society or other partner) holds exclusive rights to this article under a publishing agreement with the author(s) or other rightsholder(s); author self-archiving of the accepted manuscript version of this article is solely governed by the terms of such publishing agreement and applicable law.